JMEPEG (2018) 27:764–776
https://doi.org/10.1007/s11665-017-3107-7

1059-9495/$19.00

Laser-Hardened and Ultrasonically Peened Surface Layers on Tool Steel AISI D2: Correlation of the Bearing Curves' Parameters, Hardness and Wear

D.A. Lesyk, S. Martinez, B.N. Mordyuk, V.V. Dzhemelinskyi, A. Lamikiz, G.I. Prokopenko, K.E. Grinkevych, and I.V. Tkachenko

(Submitted June 27, 2017; in revised form November 7, 2017; published online December 22, 2017)

This paper is focused on the effects of the separately applied laser heat treatment (LHT) and ultrasonic impact treatment (UIT) and the combined LHT + UIT process on the wear and friction behaviors of the hardened surface layers of the tool steel AISI D2. In comparison with the initial state, wear losses of the treated specimens after long-term wear tests were decreased by 68, 41, and 77% at the LHT, UIT, and combined LHT + UIT processes, respectively. The Abbott–Firestone bearing curves were used to analyze the material ratio and functional characterization (bearing capacity and oil capacitance) of the studied surface specimens. The wear losses registered after short (15 min) tests correlate well with the changes in experimental surface roughness *Ra*, and the predictive *Rpk*, and bearing capacity B_C parameters, respectively, evaluated using the Abbott–Firestone curves and Kragelsky–Kombalov formula. The wear losses after the long-term (45 min) tests are in good correlation with the reciprocal surface microhardness *H*V and with the W_L and W_P wear parameters, respectively, estimated using Archard–Rabinowicz formula and complex roughness-and-strength approach. The observed HV increase is supported by nanotwins (LHT), by dense dislocation nets (UIT), and by dislocation cells/nanograins fixed with fine carbides (LHT + UIT) formed in the surface layers of the steel.

Keywords bearing curve, hardness, laser heat treatment, tool steel AISI D2, ultrasonic impact treatment, wear

1. Introduction

The quality of the surface layers of products is one of the important characteristics affecting their operational properties, such as corrosion and wear resistance, stiffness contact/bearing capacity, and fatigue life. The enhanced surface quality is provided both by low surface roughness and by improved physical and mechanical properties of the material (Ref 1). Advanced technological processes applied to the material surface may reduce financial and energy expenses owing to use of the modified surface materials instead of more expensive bulk materials of high strength in the machine parts production.

D.A. Lesyk and **V.V. Dzhemelinskyi**, Department of Laser Systems and Applied Technologies, National Technical University of Ukraine "Igor Sikorsky Kyiv Polytechnic Institute", 37 Peremohy ave., Kiev 03056, Ukraine; **S. Martinez** and **A. Lamikiz**, Department of Mechanical Engineering, University of the Basque Country, Alameda Urquijo s/n, 48013 Bilbao, Spain; **B.N. Mordyuk** and **G. I. Prokopenko**, Department of Physical Fundamentals of Surface Engineering, G.V. Kurdyumov Institute for Metal Physics, NAS of Ukraine, 36 Academician Vernadsky blvd, Kiev 03680, Ukraine; and **K.E. Grinkevych** and **I.V. Tkachenko**, Department of Physics of Metastable Alloys and High-Strength Materials Destruction, Frantsevich Institute for Problems of Materials Science, NAS of Ukraine, 3 Krzhizhanovsky str, Kiev 03680, Ukraine. Contact e-mails: lesyk_d@ukr.net and mordyuk@imp.kiev.ua.

The surface coating processes are known to be effective in improvement of the surface properties of details (Ref 2). However, the obtained coatings may undergo failure, wear, and delaminations at severe mechanical loads, high motion speeds, high specific contact pressures, and thermal cycling. Thus, the other approaches for the modification of the surface microrelief and microstructure without changing the chemical composition can be demanded (Ref 3). Additionally, traditional thermal treatment cannot always be able to provide the required quality of materials. Therefore, the actions of highly concentrated energy sources, such as plasma, electron beam, or laser, which allow rapid heating/cooling of the irradiated near-surface layers, can be used for effective thermal hardening of the material surface (Ref 1, 4).

Particularly, the plasma hardening allows obtaining deep and wide heat-affected zones, and it is relatively cheap and high-performance process (Ref 5). Surface hardening produced by the actions of the electron (Ref 6) or laser (Ref 7, 8) beams is characterized by high stability, and the thermal effects on the treated materials can be either local or extensive. The main advantage of the laser heat treatment (LHT) for surface hardening is a possibility to perform the treatment in the environment air, while the action of electron beam requires the vacuum conditions (Ref 9). The LHT process using modern laser technological systems, such as high-power diode laser or fiber laser with scanner optics, ensures high accuracy and performance of the hardening process, and it allows obtaining the high-quality surfaces.

A number of methods for mechanical hardenings, such as ball burnishing (Ref 10) or roller burnishing (Ref 11), shot peening (Ref 12), ultrasonic finishing treatment (Ref 13), or ultrasonic impact treatment (UIT) (Ref 14), are known to induce severe

plastic deformation (SPD) in the surface layers of the treated materials. Normally, the SPD processes occurred through the marked structural changes associated with generation/interaction of dislocations/twins, and with the grain refinement. Additionally, it is accompanied by the formation of macro- and microstresses (Ref 15). The UIT process was shown to be one of the most effective methods of the surface modification. Particularly, it results in relatively thick severely deformed near-surface layers and the formation of the regular wavy surface microrelief with high oil holding capacity. Additionally, it has good controllability and can be easily automated (Ref 16).

The combined thermo-deformation processes, which may include the highly concentrated energy of arc plasma, electron or laser beams, and the methods of severe plastic deformation seem promising in surface hardening and improving the surface-related properties, such as corrosion, wear resistance, and fatigue resistance (Ref 17). Recently, the combined LHT + UIT process was considered (Ref 18), which was consisted of the laser transformation hardening [the LHT process characterized by high rates of local heating (10^{10} °C/s) and cooling (10^{6}…10^{8} °C/s)] and subsequent strain hardening by severe plastic deformation induced by multiple impact loads at the UIT process (with the strain rate of $\sim 10^{3}$ s^{-1}). It was shown the result in the highest quality properties of the surface layer in comparison with those achieved by means of the LHT or UIT processes used separately (Ref 19). Wear and tribological characteristics of metallic surfaces were shown can be successfully assessed by using the bearing curves of the surfaces (Ref 20) and bearing ratio parameters (Ref 21).

The purpose of this work is twofold. The reduced wear of the tool steel AISI D2 is aimed to be achieved by means of the combined laser heat treatment and ultrasonic impact treatment. Additionally, the relationships between the wear losses and the profile topographic parameters of the surface microrelief and microhardness of the surface layer are aimed to be established.

2. Experimental Procedures

2.1 Material

High-chromium tool steel AISI D2 studied in this work is widely used in mechanical engineering for production of tools and components that work at significant dynamic loads, such as dies, punches, rollers. Their surface layers should normally be of high quality and operational properties. Plane specimens of this steel (dimensions 69 mm × 69 mm × 9 mm) were initially heated to 850 °C, then slowly cooled in the furnace to 650 °C (10 °C per hour), and then cooled in the environment air. The specimens were milled before surface treatments (the initial surface roughness was $\sim Ra = 2.5$ μm). The chemical composition and mechanical properties of the studied steel are listed in Tables 1 and 2.

The magnitudes of the surface hardness and microhardness randomly measured on the surface and averaged are also given in Table 2.

2.2 Laser Heat Treatment

Laser heat treatment (LHT) for remote hardening of the specimen surface was performed using the equipment assembled on the base of a Kondia Aktinos B500 machine with computerized numerical control (CNC) shown in Fig. 1(a). A Rofin Sinar FL010 fiber laser with a maximum power output of 1 kW ensured cylindrical spot of ∼ 1 mm in diameter and multimode energy distribution in the focal plane. A Scanlab Hurry Scan 25 with galvanometric scanner head, special devices, and software allow obtaining a large spot area owing to fast oscillation of the laser beam in two directions (the scanning speed V_{sc} and the scanning width h_{sc} determine to the track width b_{sc}) (Fig. 1b) (Ref 19, 22).

A strategy of maintaining constant temperature under the laser beam was chosen for the LHT studied in this paper. The constant temperature strategy allows to avoid undesirable overheating or melting of the treated surface if the thickness, slope, or roughness of the specimen (workpiece) would be changed. An Impac Igar 12LO two-color pyrometer was used to the real-time measurements of the temperature in the zone irradiated by the laser beam. A proportional-integral-differential (PID) controller was used to change the laser power needed to maintain the temperature in the working area to be constant (Fig. 2) (Ref 23). The LHT process was monitored and recorded in real time using a high-speed camera (Fig. 1a).

The LHT process was carried out in the environment air at a scanning speed $V_{sc} = 1000$ mm/s, scanning width $h_{sc} = 10$ mm, and the specimen feed rate $S = 90$ mm/min, which provided a duration of the laser action on the treated area unit $t_l \approx 0.66$ s and the heating temperature $T = 1270$ °C.

The complete austenitization temperature range was estimated by the ternary iron–carbon–chromium phase diagram that took the chemical composition of the material as well as the thermo-kinetic and thermo-physical models into account (Ref 24-27). The aforementioned methods allow accounting for the limiting maximum heating temperature ($A_{C3} < T$ (°C) $< T_m$) and duration of the laser action ($0.01 < t_l$ (s) < 1.5) that provided a thermal hardening without melting the surface. The duration of the laser action t_l was determined by the ratio of the diameter d_{lb} or length l_{lb} of the laser beam (mm) and the specimen feed rate S (mm/s). The heat energy of the laser beam was determined by the ratio of laser power (W) and the laser beam diameter (mm) and the specimen feed rate (mm/s). In this study, the calculated magnitude of spent energy at the LHT process for the laser surface hardening was ∼ 40 kJ/cm^2 that allowed carrying out the laser heat treatment without melting of the surface layer and simultaneously ensuring the hardening depth of ∼ 0.3 mm.

2.3 Ultrasonic Impact Treatment

The UIT process was carried out at ambient temperature using the equipment and regimes described earlier (Ref 15, 19). The UIT equipment, which contained an ultrasonic generator with a frequency f_{usv} of 21.6 kHz and a power output of 0.3 kW, the ultrasonic vibrating system with a piezoceramic transducer, step-like horn, and the impact head with seven cylindrical pins,

Table 1 Chemical composition of the tool steel AISI D2 (wt.%)

C	Cr	Mo	V	Mn	Si	Ni	Cu	P, S	Fe
1.55	11.3	0.83	0.72	0.46	0.42	0.15	0.06	< 0.03	Bal.

Table 2 Mechanical properties of the tool steel AISI D2

σ_Y (MPa)	σ_U (MPa)	δ (%)	E (GPa)	μ	HRC_1	$HV_{0.05}$ (GPa)
≥ 320	≥ 710	≥ 16	200	0.25	19.6	3.2

σ_Y is the tensile yield strength, σ_U is the tensile ultimate strength, δ is relative elongation, E is the Young's modulus, μ is Poisson's ratio, HRC is the surface hardness, $HV_{0.05}$ is the microhardness in the specimens' cross sections

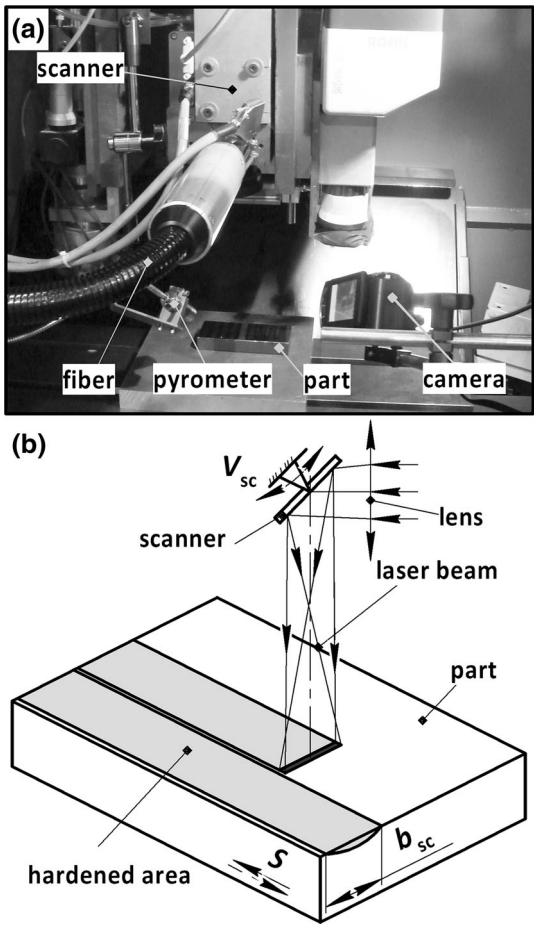

Fig. 1 General view of equipment (a) and scheme (b) of the LHT process for remote surface hardening: V_{sc} is the scanning speed, b_{sc} is the track width, and S is the specimen feed rate

was assembled in the CNC machine and loaded onto the treated surface with a static force $F_s \approx 50$ N (Fig. 3a). The used vibration amplitude A_{usv} of ultrasonic horn tip was ~ 18 μm. These ultrasonic vibrations induced stochastic impacts of the pins by the treated surface, and the frequency f_i of these induced impacts was ~ 3 ± 0.5 kHz. During the UIT process, the impact head was forcedly rotated (the rotation speed was ~ 76 rpm) to induce the shear constituents of the impacts (Ref 19). The ultrasonic system was moved along the treated surface at a speed $S = 600$ mm/min. The UIT process lasted for 120 s provided relatively high coverage of the treated area: The specific number of impacts was ~ 400 imp/mm^2. The mechanical energy of the ultrasonic tool used was estimated to be ~ 160 kJ. The experimentally measured temperature increase at the UIT process did not exceed ~ 150 °C.

2.4 Examinations of Topography of Surface Relief, Microstructure, and Microhardness

The surface roughness, microrelief topography, and Abbott–Firestone material ratio curve were investigated using optical microscope/profilometer Leica DCM3D with 10XLD confocal lens and appropriate software. To characterize the surface roughness, both the traditional parameters, such as arithmetic mean roughness parameter *Ra* and total height *Rt* of the roughness profile, and a number of functional parameters (*Rpk*, *Rk*, *Rvk*) of the surface profile (Fig. 4d) were evaluated according to the ISO 13565-2 standard (Ref 28). Analysis of the 2D texture of the microrelief of the surface area of 2.5 × 3 mm (Fig. 4a and b) and the bearing curve (the Abbott–Firestone material ratio curve) coupled with the histogram of the profile depths of the surface roughness (Fig. 4c) was carried out in accordance with the ISO 4287 standard.

Using the Abbott–Firestone curve and profile bearing curve of surface roughness profile (Fig. 4d), the following functional parameters of the surface roughness profile were graphically evaluated (Ref 29): *Rpk* is the average arithmetic height of peaks on the top of the surface roughness profile of microrelief; *Rk* is the average arithmetic depth of the core of the surface roughness profile (limited by the upper and lower horizontal lines); *Rvk* is the average arithmetic depth of the valleys on the bottom of the surface roughness profile; Mr_1 and Mr_2 are the material ratios, respectively, obtained by the intersections of the upper and lower horizontal lines and Abbott–Firestone curve, which are, respectively, related to the highest outstanding peaks and the deepest valleys out of the core of surface roughness profile.

Additionally, the surface microreliefs of the original and modified specimens were analyzed by the scanning electron microscopy (SEM) using JSM 6490LV microscope.

The analysis of the microstructure in the near-surface layers was carried out using Nikon Optiphot-100 optical microscope and transmission electron microscopy (TEM) and selective area electron diffraction (SAED) applying a JEOL CX-II JEM100 microscope. Additionally, the x-ray diffraction (XRD) analysis of the surface layers was carried out using a DRON-3 M diffractometer to assess the treatment-induced macrostresses using a $\sin^2\psi$-based method and literature values of elastic modulus and Poison's ratio.

Microhardness of near-surface layers was measured using a digital tester FM800 at a load on the Vickers indenter of 0.5 N and the dwell time of 12 s.

2.5 Experimental and Theoretical Evaluations of Wear

The wear tests were carried out using the automated tribological complex described elsewhere (Fig. 5a) (Ref 30, 31). The initial and treated specimens were tested for 15 and 45 min by the hard metal (94% WC, 6% Co) indenter (8 mm in diameter, hardness 94 HRA) performing the reciprocating sliding movement with frequency of 1 Hz and sliding speed

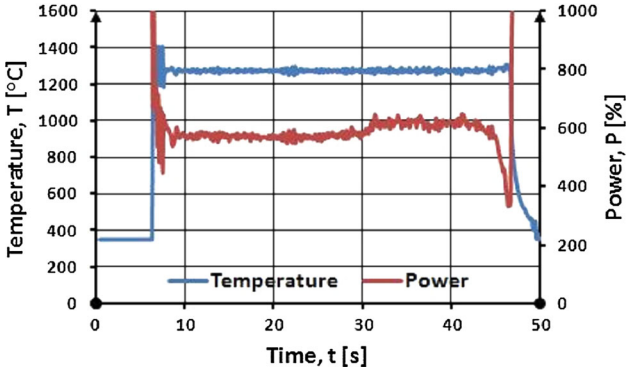

Fig. 2 Temperature (1) and laser power (2) real-time recordings registered by the automatic monitoring system

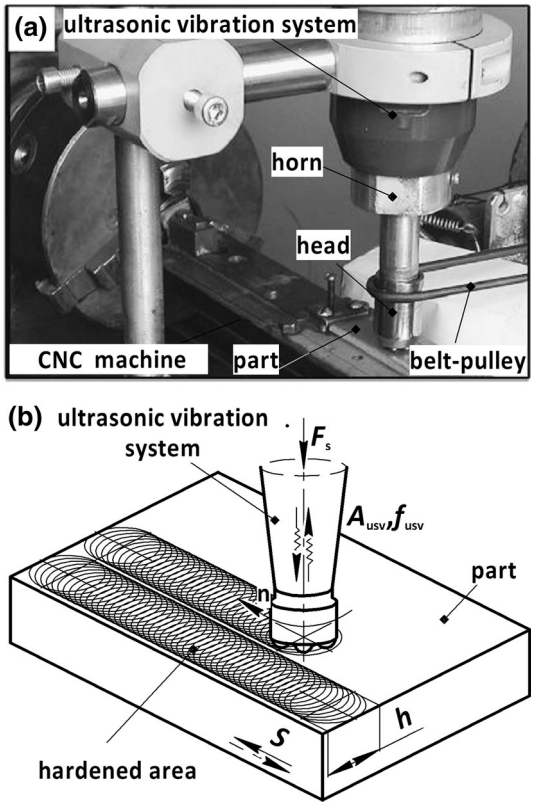

Fig. 3 General view of the UIT equipment (a) and scheme of the UIT process (b): F_s is a static load, A_{usv} and f_{usv} are the vibration amplitude and frequency of ultrasonic horn tip, S is the feed rate of specimen, and h is the track width

$\sim$ 0.013 m/s along the track of 4 mm long on flat specimen surfaces in the industrial oil *I*20 at a constant load $F_s = 30$ N, which was chosen based on the mechanical properties of the investigated specimens. Frictional force F_f was estimated using the tensometer measuring the displacement of the elastic element that was inelastically connected to the tested specimen (Ref 30). The magnitude of wear loss W_L was determined by the profile (Fig. 5b and c) and topography (Fig. 5d) as the depths of the worn track using an optical profilometer Leica DCM3D.

The theoretical assessment of bearing capacity B_C of the surface microrelief of the treated specimens was carried out based on the relation between the profile parameters and surface roughness topography by means of Kragelsky–Kombalov formula (Ref 32):

$$B_C = \left(\frac{100}{t_m}\right)^{1/v} \cdot \left(\frac{Rp}{\rho_m}\right), \quad \text{(Eq 1)}$$

where t_m is the relative bearing length of the microasperities of the surface roughness profile at the middle line (%), v is the parameter calculated as $v = 2t_m(Rp/Ra) - 1$, where Ra is the arithmetic mean deviation of the roughness profile (μm), Rp is the maximum profile peak height of the roughness profile (μm), ρ_m is the average radius of the microasperities' peaks of the surface roughness profile (μm).

The theoretical magnitude of the wear losses W_L was estimated by Archard–Rabinowicz equation describing the inverse proportionality of wear and microhardness of the tested material (Ref 30):

$$W_L = \frac{KF_s l}{HV}, \quad \text{(Eq 2)}$$

where K is the wear coefficient, F_s is the static load (N), l is the length of the worn track (mm), *and* HV is the microhardness of the tested material (N/mm^2).

To perform the complex evaluation of the quality of the product surface layer, particularly the wear resistance, both the surface microrelief parameters (parameters of roughness, waviness, and macrodeviation) and the physical/mechanical properties of the surface layer (the hardening intensity, residual stresses etc.) should be taken into account. In this study, one of such complex approaches is used for theoretical estimation of the wear resistance, and the wear parameter W_P was evaluated in accordance with the following formula (Ref 32):

$$W_P = \frac{(Ra \cdot Wz \cdot Ht)^{1/6}}{t_m^{3/2} \cdot Sm^{1/2} \cdot I_{hard}^{2/3} \cdot \lambda}, \quad \text{(Eq 3)}$$

where Ra is the arithmetic mean deviation of the surface roughness profile within a sampling length (μm), Wz is the average height of the surface waviness profile within a sampling length (μm), Ht is the maximum macrodeviation (μm), t_m is the relative bearing length of the microasperities of the surface roughness profile at the middle line (%), Sm is the average step between the microasperities of the surface roughness profile at the middle line (mm), I_{hard} is the hardness intensity of the surface layer, which can be calculated as the ratio of the hardness increment in the hardened layer to the initial material hardness $\left(I_{hard} = (H_\mu^{hard} - H_\mu^{in})/H_\mu^{in} \cdot 100\%\right)$, $\lambda = [(\sigma_U - \sigma_R)/\sigma_a]^{t_y}$ is the parameter accounting for the stress state of the tested material, σ_U is the tensile ultimate strength of material (MPa), σ_R is the residual microstresses (MPa) (Ref 19), σ_a is the applied stress acting on the friction surface (MPa), which is calculated by Hertzian theory of non-adhesive elastic contact, and t_y is the parameter accounting for the friction fatigue at elastic contact [t_y ranges from 3 to 14 (Ref 33)].

3. Results and Discussion

A friction and wear are known to significantly depend on both the sliding conditions and properties of contacting

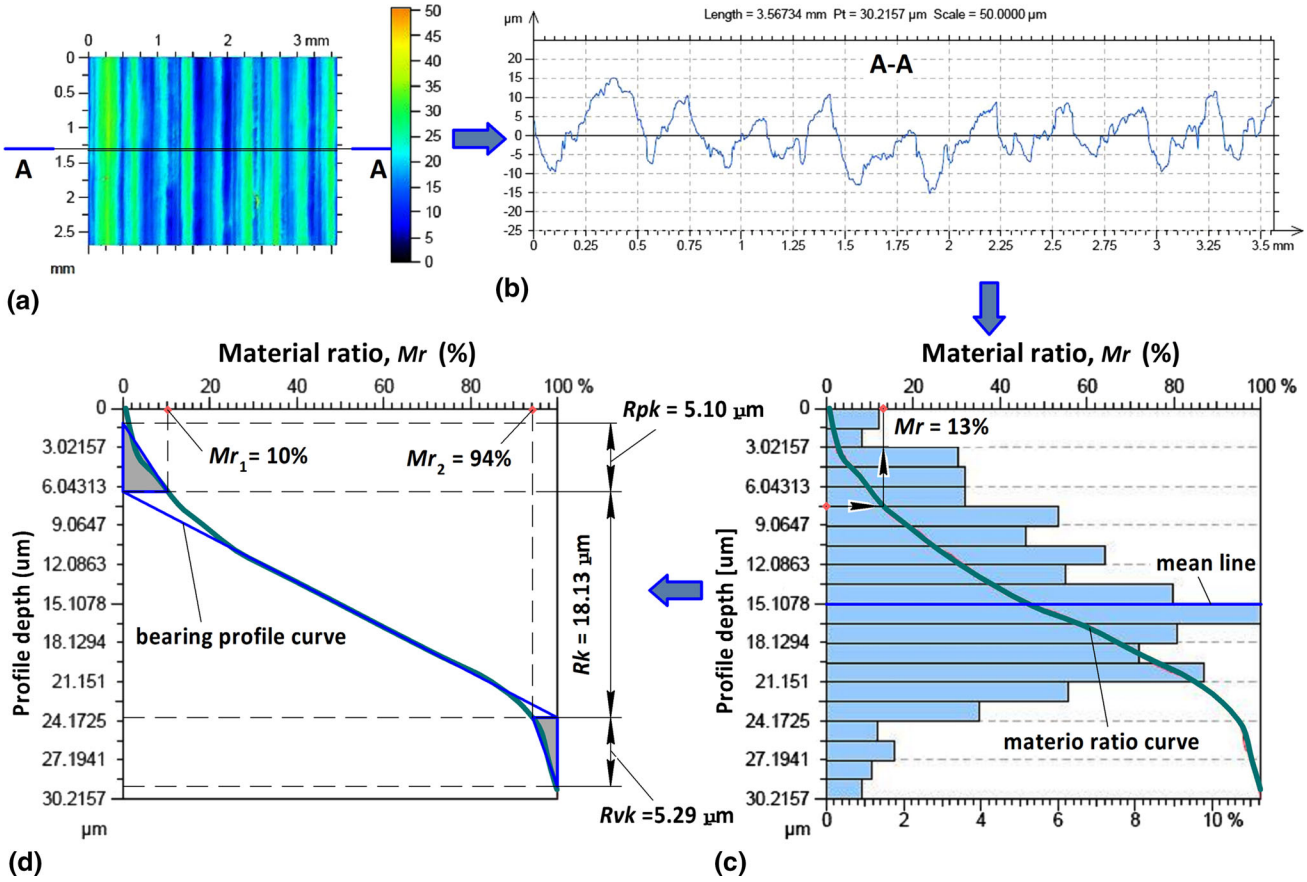

Fig. 4 Two-dimensional surface texture (a), surface roughness profile (b), material ratio curve coupled with the depths' histogram of the surface roughness profile (c), and definitions of the functional parameters of the surface roughness profile (d)

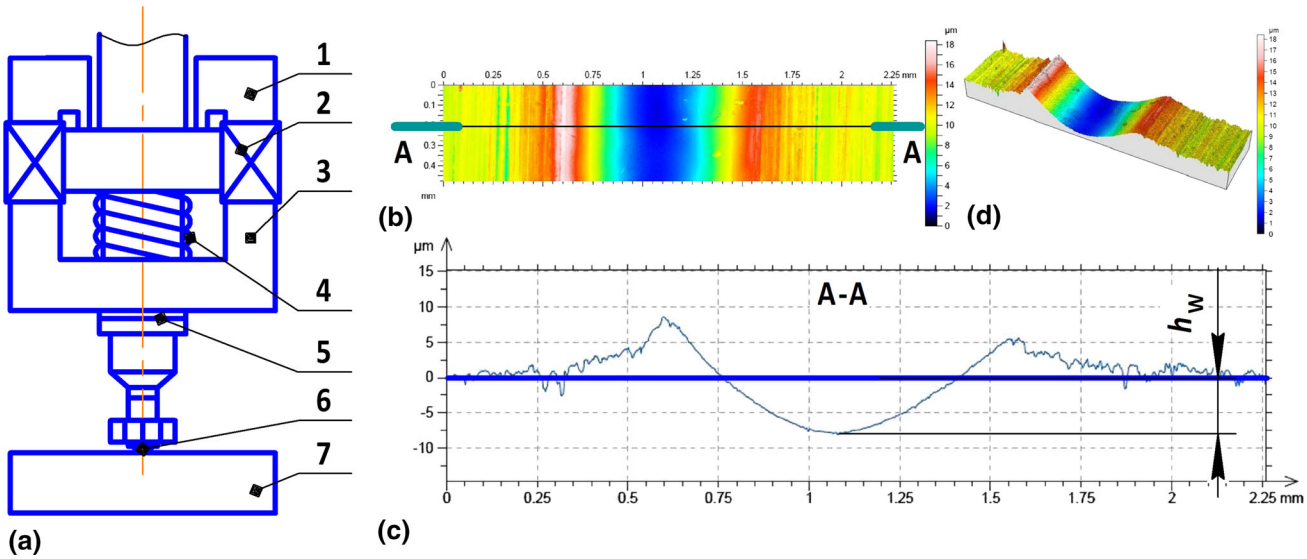

Fig. 5 Scheme of the automated tribological complex (a) consisting of frame (1), coil (2), electromagnet (3), electromagnet (4), lock ring (5), indenter (6), and treated surface (7); 2D surface texture (b), profile (c), and 3D surface texture (d) of the worn track: h_W is the measured wear magnitude

materials. The former includes the normal load and sliding speed, and the latter comprises the surface topography described by the roughness parameters and mechanical properties (primarily hardness) of the surface layer (Ref 34). One of the first theoretical predictions of materials' wear was reported by Holm, who established that the quantity of the material

removed by wear depends on the ratio of sliding length to the real contact area of two rough surfaces. The contact area can be adequately described by so-called material ratio *Mr*, which magnitude is largely determined by the parameters of the surface roughness (Ref 35). It was established that the reduction in the roughness parameters of the surface microrelief is not always beneficial for lowering the friction force and wear losses (Ref 28, 36). According to the molecular-mechanical theory of friction by Kragelsky accounted for the dual nature of the friction force, the surface finishing (reduction in the surface roughness) results in the decrease of the mechanical (abrasive) constituent of friction and in the simultaneous increase of adhesive constituent of friction (Ref 36). On the other hand, according to the well-known Archard–Rabinowicz equation (Eq 2), the magnitude of the worn material (W) is inversely proportional to the hardness of the tested surface and directly proportional to the sliding length, applied load, and wear coefficient (Ref 37). Therefore, it seems reasonable to use the combined assessment methods that will take the roughness parameters of the surface microrelief and mechanical properties into account simultaneously. The complex parameter W_P of such type, which was described by Eq 3, is also used in this study.

3.1 Parameters of Surface Microrelief

The appearance of the surface microreliefs of the specimens of the tool steel AISI D2 was observed using SEM analysis. Figure 6 shows changes in the surface morphologies induced by different surface modification methods used in this study. Many parallel grooves visible on the roughly polished surface of the original specimen (Fig. 6a and b) became masked by the oxide film formed after LHT, and the surface appears less rough (Fig. 6c). Higher magnification allows revealing many cracks of various sizes probably formed during the heating–cooling cycle owing to the difference in the thermal expansion coefficients of the steel and oxide. A rather smooth and wavy surface is observed due to plastic deformation in the case of the UIT-processed specimen (Fig. 6e). However, a closer examination shows that it still contains some unsmoothed areas in the sites of the deepest initial grooves (Fig. 6f). The LHT + UIT-processed surface is also fairly smooth. However, in this case, there are additional small elements, which look like the imparted hard particles in the matrix surface (Fig. 6g). These particles formed due to UIT-induced fracturing of the LHT-hardened microasperities promote additional smoothing of the resulting surface microrelief of the LHT + UIT-processed specimen (after finishing UIT) (Fig. 6g and h) owing to their abrasion effect.

Results of more precise analysis of the surface profiles of the steel specimens in the initial state and after different treatments are shown in Fig. 7. Traditional parameters describing the surface roughness, such as *Ra* or *Rt*, shown in Fig. 8(a) not always allow assessing the possible operational properties of the surface microrelief studied. Conversely, a number of functional parameters (*Rpk*, *Rk*, *Rvk*) of the surface profile, which can be obtained by means of the nonparametric estimations of the shape of the roughness profile using the Abbott–Firestone curve and profile bearing curve, can be very useful in predicting the operational properties of the surface microrelief, for instance, the wear behavior at different stages of the detailed exploitation (Ref 38). Thus, all the profiles shown in Fig. 7 are accompanied with the results of their analyses carried out in the framework of the Abbott–Firestone approach (Ref 32). Plotting the profile bearing curves and probability histograms allows determining the aforementioned functional

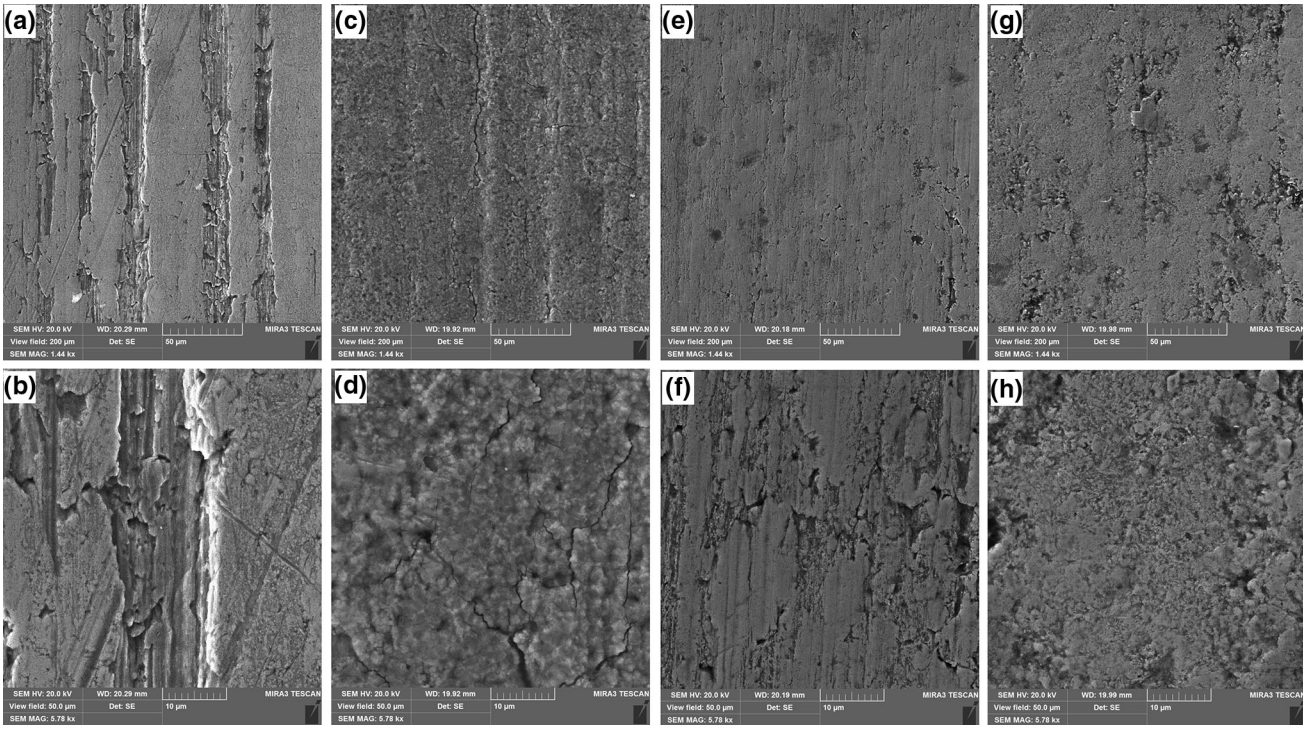

Fig. 6 SEM observations of the surface microreliefs of the specimens of tool steel AISI D2 in the initial state (a, b) and after LHT (c, d), UIT (e, f) and combined LHT + UIT (g, k) processes

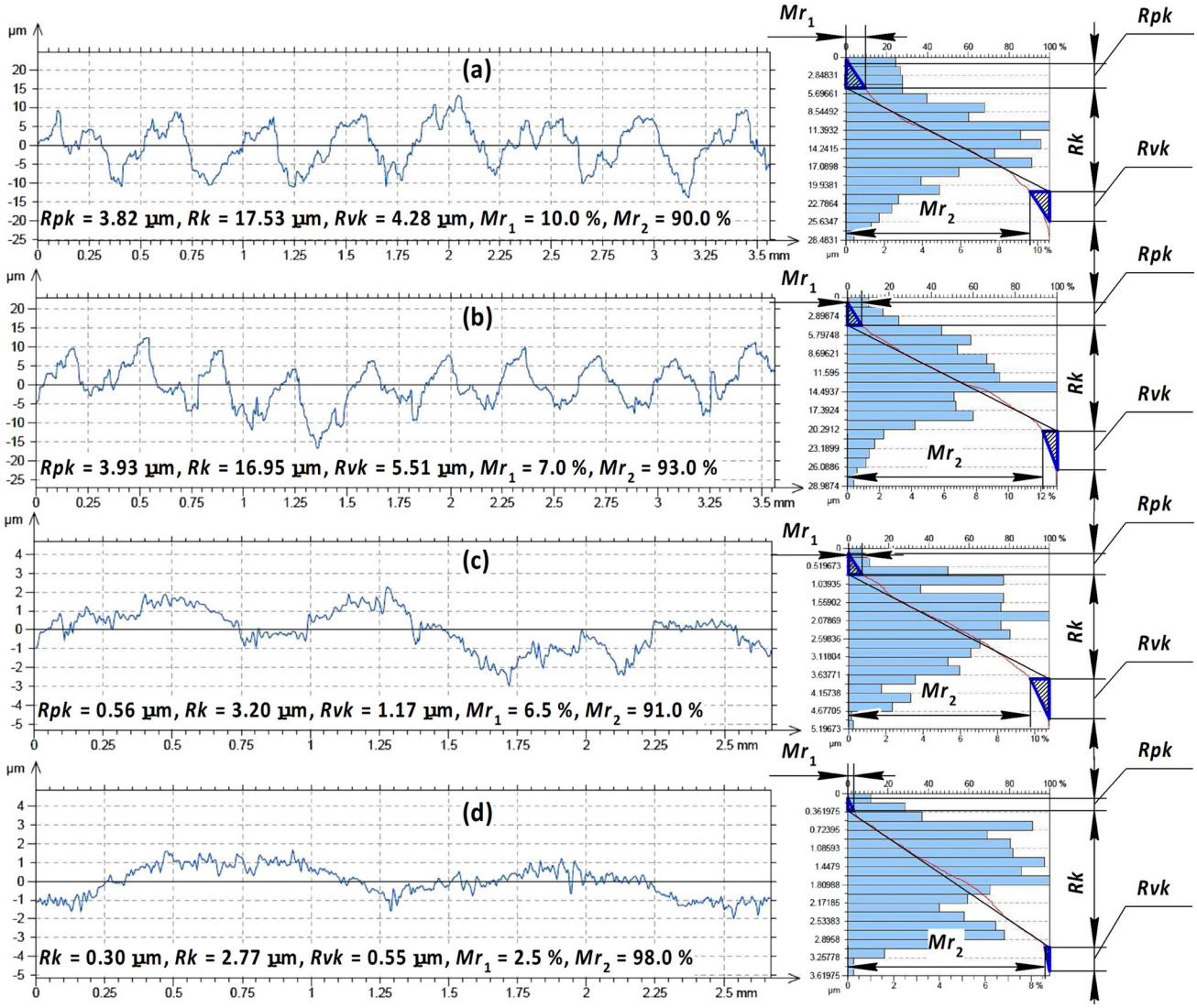

Fig. 7 Two-dimensional surface profiles of the specimens of tool steel AISI D2 in the initial state (a) and after LHT (b), UIT (c) and combined LHT + UIT (d) and graphical evaluations of functional parameters *Rpk*, *Rk*, *Rvk*, and material ratios *Mr* using the Abbott–Firestone curve and profile bearing curve of the surface roughness

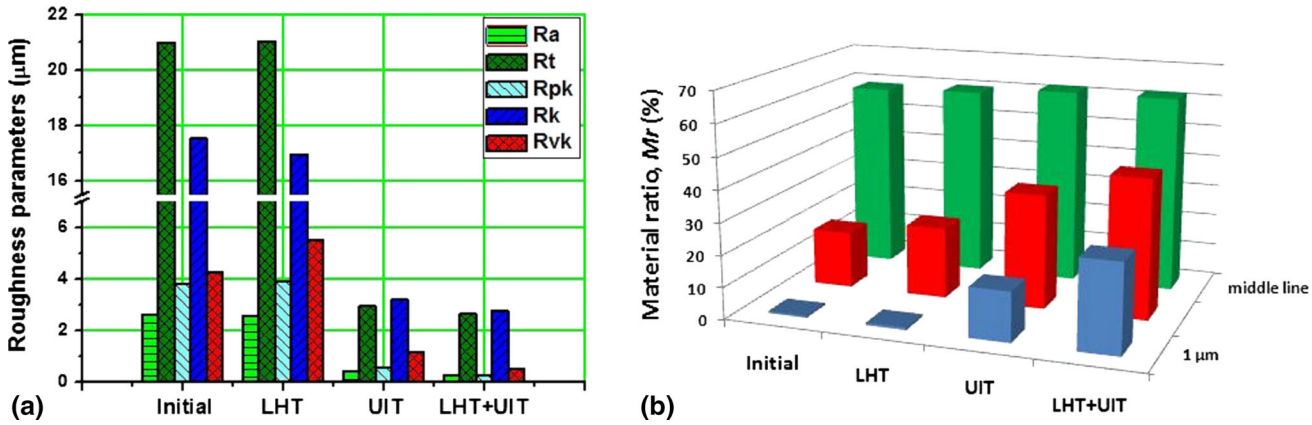

Fig. 8 Surface roughness (*Ra*, *Rt*) and bearing curve (*Rpk*, *Rk*, *Rvk*) parameters (a) and the magnitudes of the material ratio *Mr* (b) of the tool steel AISI D2 in the initial state and after the LHT, UIT, and combined LHT + UIT processes

parameters of the profiles observed after various treatments. The changes in these parameters are also shown in Fig. 8(a).

Experimental studies of the surface microrelief (Fig. 7) show that the LHT process has an insignificant effect on the surface roughness and functional parameters due to lack of melting of the surface layer. Conversely, the UIT process applied the rotating impact head leads to significant changes in the surface roughness caused by severe plastic deformation of the surface layers induced by multiple sliding impacts of high frequency (Ref 19), as a result, the improved microrelief with the diminished roughness albeit slightly increased waviness is formed. Considering the modification extent of the surface microrelief, the combined LHT + UIT process, viz. the laser-ultrasonic hardening/finishing technology, appears the most effective in comparison with the separately used LHT or UIT processes.

The combined LHT + UIT process results in the most significant improvement in the roughness parameters. In this case, the preliminarily performed laser thermal hardening of the surface facilitated the destruction of the hardened microasperities at subsequent UIT process despite some reduction in the plastic strain extent (and thickness) of the deformed layer. As a result, the combined process allows obtaining minimum magnitudes of the roughness parameters (Fig. 6, 7d, and 8a).

In this study, all the identified functional parameters of the surface profiles of the AISI D2 steel specimens demonstrate similar behavior irrespective of the treatment used. They are insignificantly changed after LHT and essentially reduced after the UIT and combined LHT + UIT processes. Considering the estimated wear magnitude in the aforementioned profile running-in stage, the *Rpk* parameter is the most important. Conversely, the *Rk* parameter allows predicting the wear resistance of the part at the long-term operation. Both the untreated and the LHT-processed surfaces are characterized by the relatively large magnitude of initial wear losses on the profile running-in stage (Fig. 8a), but the LHT-processed surface is evidently more wear resistant. After the UIT and combined LHT + UIT processes, both *Rpk* and *Rk* are significantly reduced. The combined LHT + UIT process results in more than five times reduction in the parameters *Rpk* and *Rk* (*Rpk*) in comparison with those for the initial surface. It allows predicting the increased wear resistance of the microrelief obtained. Thus, the combined LHT + UIT process promotes a quicker formation of the equilibrium roughness (the profile running-in stage becomes shorter) and facilitates enhanced wear resistance on the long-term operation stage. A correlation between the decreased *Rpk* and *Rk* and the increased material ratio *Mr* parameters on the various depths from the treated surface is observed (Fig. 8b). Furthermore, considering both the UIT-processed and LHT + UIT-processed surfaces, the parameters *Rvk* and *Mr* indicate their high oil holding capacity, which although are lesser than those observed in the original and LHT-processed surfaces having numerous valleys with high oil holding capacity (Ref 39). Owing to the deformation/destruction of the microasperities during the UIT process, the material ratio *Mrs* for the highest peaks of the surface roughness profile is increased more than eight times in comparison with the untreated surface (Fig. 6, 7, and 8b). Experimental studies (Ref 40, 41) also show that severe plastic deformation of the alloyed steel by means of shot peening allowed to obtain two times reduction in functional parameters and to increase the *Mrs* in 4-8 times depending on the treatment duration (1…15 min). The magnitude of the *Mrs* after the combined LHT + UIT process is much higher (*Mrs* = 28%) than that for the untreated surface (*Mrs* = 0.6%). It can also be an indicator of a much longer lifetime of the LHT + UIT-processed surface (Fig. 8).

3.2 Microstructure Examination

Microstructures formed in the surface layers of the steel specimens after different processes used for surface modification are shown in Fig. 9. All of the microstructures registered by optical microscopy contain large strip-like carbides, which support high hardness of the steel. A heat-affected zone (HAZ) is clearly visible after LHT and LHT + UIT as the slightly darker areas (their boundaries are marked with the red arrows in Fig. 9a and g). The thickness of the HAZ is ~ 300 μm. The surface relief appears to be unchanged after LHT. On the contrary, the UIT process inducing severe plastic deformation of the surface layer results in a wavy surface. The strain-affected zone (SAZ) formed after UIT and marked by the blue arrow in Fig. 9(d) is thinner (~ 50 μm). In the case of the combined LHT + UIT process, some exfoliations and cracks are visible on the top surface additionally to the LHT-induced HAZ and UIT-induced SAZ (see white arrows in Fig. 9g and h). They can be caused by a higher hardness of the LHT-processed surface layer and disappear after long UIT processing. As a result, the surface roughness parameters are much lower than those of the original and LHT-processed specimens (Fig. 6, 7, and 8).

More precise analysis of the microstructures carried out by TEM observations of the top surface layers (Fig. 9c, f, and k) shows a number of distinctive features. Nanotwins and/or martensitic nanolathes were formed in the top surface of the LHT-processed specimen (indicated by yellow arrows in Fig. 9 (c). An appropriate SAED pattern is characteristic for the twinned microstructure. Accounting for the well-known Hall-Petch relation, such a microstructure can easily support high HV and wear resistance registered for the LHT-processed surface. However, parts of destructed oxide film serving as the abrasives could accelerate the wear process. On the contrary, UIT results in the formation of dense dislocation nets fixed with fine carbides (Fig. 9f), which can also provide the increased HV magnitudes. Although the UIT caused increase in HV is naturally lower than those registered for the LHT and combined LHT + UIT processes (see curve 5 in Fig. 13). The LHT + UIT process produces the surface layer containing areas with either fine dislocation cells or nanosized grains of random orientation fixed by secondary nanocarbides (respectively, indicated with yellow and red arrows in Fig. 9k). An appropriate SAED pattern contains almost solid circles formed owing to highly azimuthally dispersed diffraction spots of alpha iron. Both observed microstructures provide the highest surface hardness of this steel after the combined LHT + UIT process.

3.3 Wear and Friction Behaviors

The wear losses registered after tribological tests were determined by means of analysis of the wear tracks using the 3D laser microscopy. After short (15 min) tests, the wear tracks for the initial and LHT-processed specimens were more visible than those appeared on the specimens tested after the UIT and combined LHT + UIT processes (Fig. 10). Besides an evident decrease in the wear losses of the treated surfaces, which will be further analyzed in detail, one can observe another important feature related to the changes in the roughness characteristics of the wear track surface. Figure 11 shows a significant diminution

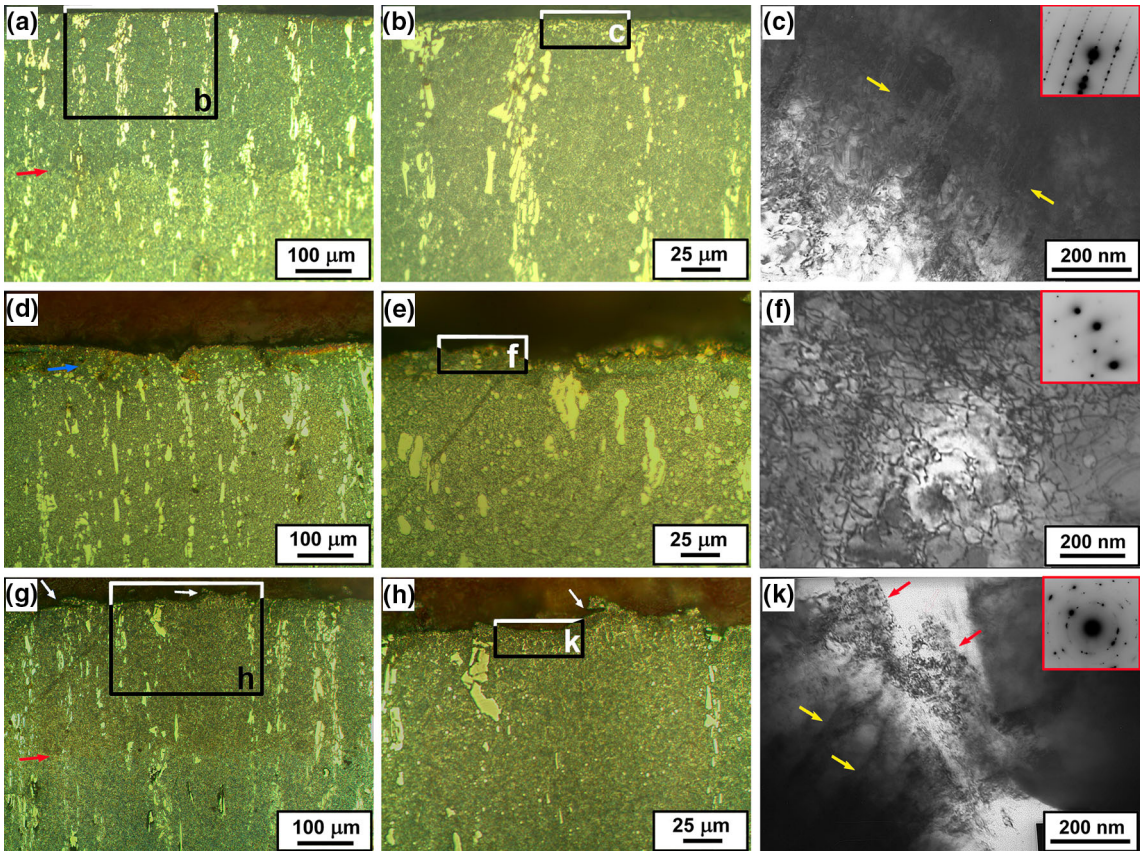

Fig. 9 Optical (a, b, d, e, g, h) and TEM (c, f, k) observations of microstructure and SAED patterns of the specimen cross sections of tool steel AISI D2 after LHT (a-c), UIT (d-f), and combined LHT + UIT (g-k) processes (Color figure online)

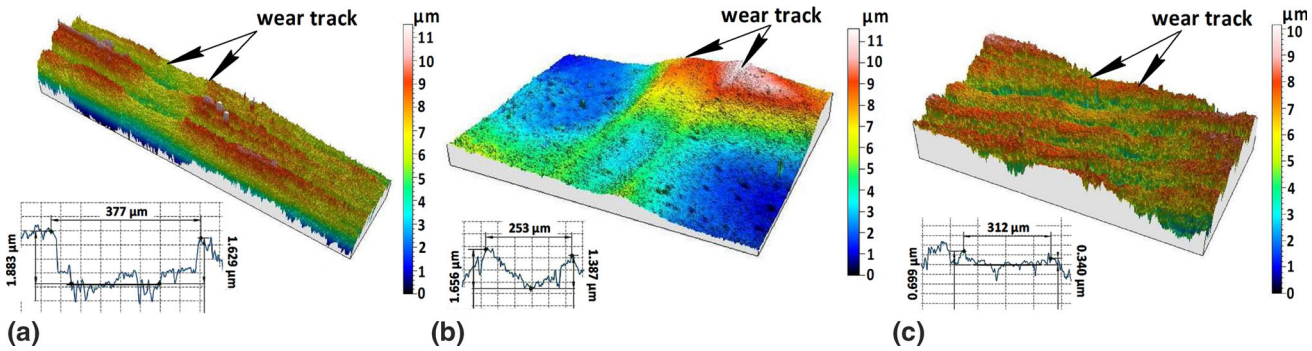

Fig. 10 3D laser micrographs of the worn tracks on the surfaces of the specimens of the tool steel AISI D2 after LHT (a), UIT (b), and combined LHT + UIT (c) after wear tests lasted for 15 min

of total heights (the R_t parameter) of the wear tracks already after short wear tests (15 min) and the R_t saturation thereafter (after longer wear tests). Thus, the surface roughness was concluded to approach the equilibrium value during this first (running-in) stage of the wear process (lasted for $\leq$ 15 min). After this running-in stage, the changes in the surface roughness was observed to be negligible.

Equilibrium roughness was shown can be either lower or higher than that of the initial roughness profiles of the contacted surfaces (Ref 32). For instance, two steel surfaces in (Ref 32) had different mechanical properties and initial roughness ($Ra_1 = 0.125$ μm and $Ra_2 = 1.35$ μm) but they got the same equilibrium roughness ($Ra_f = 0.5$ μm) when the profile running-in stage of the wear/friction process was finished. In our case, despite the essential difference between roughness parameters of the original and processed specimens, all of the specimens studied demonstrate very close surface roughness formed after short (15 min) wear tests ($Rt = 0.25\ldots0.3$ μm), and this value can be already considered as the equilibrium surface roughness. The surface roughness of the original and UIT-processed specimens becomes equilibrium quicker than that of the LHT and LHT + UIT-processed specimens, which surfaces were significantly hardened by the LHT process. It should be noted that the essential roughness decrease owing to

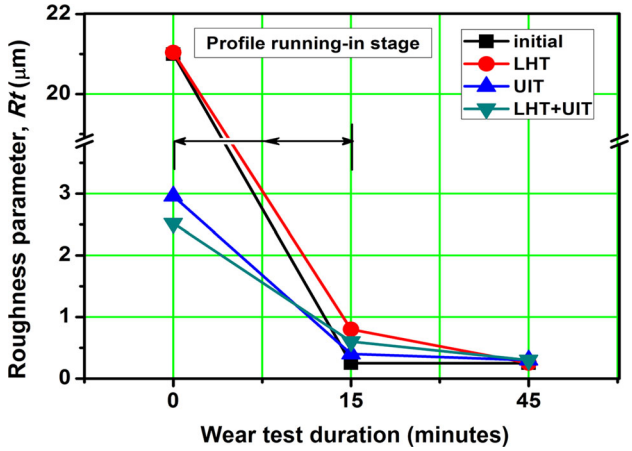

Fig. 11 Dependencies of total heights (the *Rt* parameter) of the surface roughness profiles of the tool steel AISI D2 on the duration of the wear test in the initial state and after UIT, LHT, and combined LHT + UIT treatments

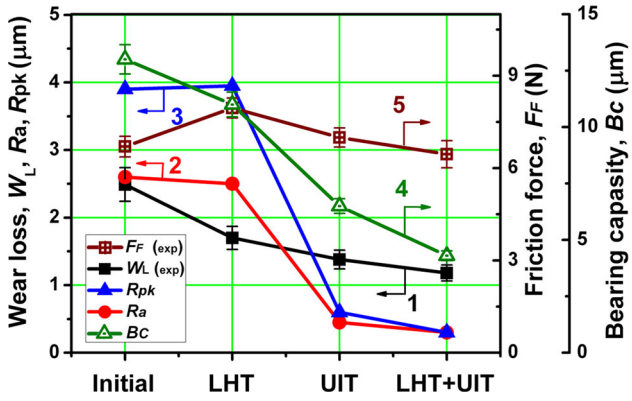

Fig. 12 Experimental wear losses W_L after wear tests for 15 min. (1), the surface roughness (*Ra*) (2), the wear value according to the Abbott–Firestone curve (*Rpk*) (3), the bearing capacity B_C of the microrelief according to Kragelsky–Kombalov formula (4), and friction force F_f (5) of the specimens of tool steel AISI D2 in the initial state and after LHT, UIT, and combined LHT + UIT

the UIT process can be considered as an additional factor facilitating the quick setting of the equilibrium roughness.

Figure 12 shows the changes in the experimental wear losses W_L (curve 1) and friction forces F_f (curve 5) of the specimens of the tool steel AISI D2 after the various treatments applied before the tests in comparison with the arithmetic roughness *Ra* (curve 2), the wear-related characteristics *Rpk* (curve 3) and B_C (curve 4), respectively, evaluated by means of the Abbott–Firestone curves (curve 3) and Kragelsky–Kombalov formula (curve 4).

On the profile 'running-in' stage, the surface roughness is known to contribute to the abrasive component of friction and thus plays the main role in the wear resistance. The behaviors of the *Rpk* and B_C parameters are in good correlation with the experimentally determined wear losses W_L. Particularly, in comparison with the initial state, the LHT, UIT, and combined LHT + UIT processes caused the decrease in the wear losses by 32, 44, and 52%, respectively. The W_L reduction after the LHT + UIT process as compared to the initial and LHT-

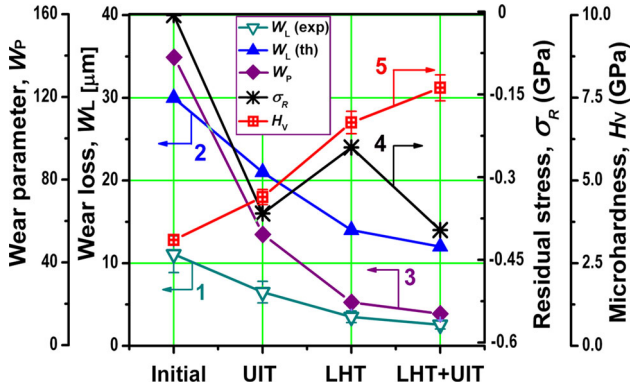

Fig. 13 Experimental wear losses after wear tests for 45 min (1), functional parameters of the surfaces of the specimens of tool steel AISI D2 evaluated using the Archard formula (2) and using the combined wear parameter W_P (3), residual stresses (4), and surface microhardness (5)

processed states can be explained by 5-8 times decrease in the *Ra* and *Rpk* parameters. The friction force F_f is markedly changed only after LHT, and the observed increase in F_f seems to be caused by high abrasion wear induced by hard broken parts of the microrelief asperities. The bearing capacity parameter (B_C) of the surface profile, which indirectly describes similar behaviors of friction/wear, is also decreased.

Evidently, when the test duration (say exploitation time) increases, the wear losses of the LHT- and UIT-processed specimens decelerate in comparison with the original one owing to the completion of the initial intensive destruction of the microasperities' peaks and owing to exhaustion of the plastic deformation because of high hardness of the specimen surface layers induced by thermal or strain hardening. In addition, the plastic deformation retards due to the strain hardening and increased material ratio in deeper sections of the surface roughness profile, i.e., the same external load becomes insufficient to produce plastic strain, but it is just able to provide some elastic deformations. To ensure the minimum wear value on the profile running-in stage, the applied treatment method should provide the resulting surface roughness, which would be close to the equilibrium one.

On the profile running-in stage, when the tested surface undertakes equilibrium roughness, both the friction and wear are mainly affected by the surface roughness formed during the manufacturing of the product (specimen) (Ref 32). At this stage, the prognosis with regard to the friction and wear characteristics is advisable to carry out using analytical approaches characterized the surface profiles, for instance, using the Abbott–Firestone curve (curve 3 in Fig. 12), or the bearing capacity B_C of the surface microrelief evaluated using the Kragelsky–Kombalov formula (Eq 1) (curve 4 in Fig. 12). On the other hand, after the formation of the equilibrium surface roughness (after the completion of the profile running-in stage), the wear losses will be mainly determined by physical/mechanical properties (hardness) of the worn surfaces, which are under consideration in the next subsection.

3.4 Correlation of Wear and Hardness

To analyze the wear characteristics after long-term tests, i.e., after the establishment of the equilibrium roughness, it is

advantageous to use the Archard–Rabinowicz expression (Eq 2) or combined approach simultaneously accounting for the characteristics of the surface profile and physical/mechanical properties of the contacted surfaces, which is described in this paper by formula (Eq 3).

Figure 13 compares the wear losses experimentally registered after the tests lasted for 45 min with the behaviors of two wear parameters theoretically evaluated using Eq 2 and 3. It is seen that the LHT-processed surfaces demonstrate higher wear resistance than those of the original and UIT-processed specimens. Particularly, the wear losses of the tool steel AISI D2 after long-term wear tests were decreased at the LHT (by 68%), UIT (by 41%), and combined LHT + UIT (by 77%) processes in comparison with those of the original specimen. This can be explained both by the deeper hardened layer formed after LHT and by higher compressive residual macrostresses in comparison with those of the UIT-processed surface (curve 4 in Fig. 13). Generally, high near-surface compressive residual stresses exert beneficial effect on the wear resistance owing to their effectiveness for the closure or at least for the prevention of the wear/fatigue cracks from opening/propagating. The surface hardness (curve 5 in Fig. 13) supported by the treatment-induced microstructural changes (Fig. 9), and compressive stresses are therefore concluded to play the main role in the wear enhancement in the long-term wear tests of specimens (longer exploitation of the product).

The LHT and combined LHT + UIT processes result in 3-4 times decrease in the wear losses in comparison with that of the original specimen, which is evidently caused both by the enhanced microhardness in relatively deep surface layer produced by the LHT process and by the decreased surface roughness (*Ra*, *Rpk*, *Rk*) induced by the UIT process. The observed efficiency is almost two times higher than that reported for the specimens of the tool steel AISI M2 subjected to high-power laser on the yttrium aluminum garnet (with Gaussian energy distribution) without scanning optics (Ref 42). Those specimens of the tool steel AISI M2 demonstrated the wear resistance, respectively, improved by 30 and 90% in comparison with the conventional thermal treatment and original specimen.

The laser surface hardening with remelting of the surface microrelief was also successfully used to decrease the surface roughness parameters of metal and alloys (Ref 43, 44) and to produce relatively thick hardened surface layers (Ref 45). Thus, specimens of the tool steel AISI D2 processed by means of the action of the continuous laser beam in optimum regime demonstrated the surface roughness parameters decreased by 80% (Ref 46). The specimens of the tool steel AISI H13 showed double enhancement in the surface microhardness (Ref 47) as compared to the original specimens after surface hardening by means of the laser treatment in nitrogen atmosphere used the 2D scanning process by the fiber laser worked in the impulsive generation mode. The laser remelting of the surface layers can often be effective in the surface roughness reduction (Ref 43) and hardness increase (Ref 48). However, the certain microstructural changes and contaminations with oxygen occurred can be undesirable in some cases. Considering these undesirable effects, the methods of severe plastic deformation, such as shot peening (Ref 41, 49), ultrasonic nanocrystal surface modification (Ref 50), or UIT (Ref 15), can be more appropriate because they can generally provide an essential hardening without contaminations and phase transformations. Both shot peening (Ref 49) and ultrasonic nanocrystal surface modification (Ref 50) techniques showed positive influence on the tribological characteristics of steels, lowered their wear rates in comparison with the original surfaces.

One of the most prospective ways for improvement of the surfaces of the steel products is to use the hybrid technologies, which may consist of rapid thermal action by the LHT process to induce the transformation hardening in the surface layers and subsequent severe plastic deformation of these surface layers by means of burnishing by balls, rollers, or pins (Ref 18). These hybrid technologies allow enhancing wear resistance and friction behavior of various steels by 20-200% owing to a double increase in microhardness caused by the structural changes consisted of dislocation multiplication, the formation of fine martensite needles and fine secondary particles of chromium-iron carbides (Ref 18) accompanied with high compressed residual stresses (curve 4 in Fig. 13).

The simultaneous application of the laser treatment (as a heating phase) and severe plastic deformation (during the cooling phase) was also shown to enhance the superficial characteristics of the steel products (Ref 24). The combined actions of continuous laser and roller burnishing of the preheated surface layer led to the formation of finer grain structures and the 30% increased wear resistance of the treated surface of the steel products. Nonetheless, may be too difficult. Therefore, the combined methods comprising sequential application of LHT and UIT addressed in this paper can be used without complex adjustment of the laser/deformation systems, and it appears to be simpler and sufficiently effective.

4. Summarizing Remarks

This paper reports on the effects of the separately applied laser heat treatment (LHT) and ultrasonic impact treatment (UIT) and the combined LHT + UIT process on the wear and friction behaviors of the hardened surface layers of the high-chromium tool steel AISI D2. Abbott–Firestone curves and bearing curves were used to analyze the material ratio and functional parameters of the studied specimen surfaces. It is shown that for the used modification methods, the surface roughness and hardness play significant roles on different stages of the wear process. The surface roughness is crucial on the initial stage (the profile running-in stage spent for the establishment of the equilibrium roughness), and the surface hardness becomes determinative on the long-term stages (say long-term exploitation of the tested material). The following important findings can be mentioned:

1. The surface roughness remains almost unchanged after single LHT ($Ra = 2.56$ μm) and is significantly diminished by the UIT ($Ra = 0.42$ μm) and combined LHT + UIT ($Ra = 0.3$ μm) processes. Similar behaviors were observed for the functional parameters (*Rpk*, *Rk*, *Rvk*) evaluated using the Abbott–Firestone curves plotted for each treated specimens. The regular microrelief formed by the combined treatment would provide the high oil capacitance of friction surfaces.
2. In comparison with the original specimens, the magnitudes of the surface microhardness were increased after the LHT (2 times), UIT (by 50%), and combined LHT + UIT (∼ 2.5 times) processes. The observed

microhardness increase is supported by nanotwins (LHT), by dense dislocation nets (UIT), and by dislocation cells/-nanograins fixed with fine carbides (LHT + UIT) formed in the surface layers of the steel.

3. The wear losses of the treated specimens experimentally registered after short tests (15 min) correlate well with the arithmetic roughness *Ra*, with the predictive magnitudes of the *Rpk* parameter, and bearing capacity B_C parameter, respectively, evaluated using the Abbott–Firestone bearing curves and Kragelsky–Kombalov formula. The surface roughness is therefore concluded to be responsible for the wear behavior on the initial stage of the wear process (the profile running-in stage).
4. The wear losses of the treated specimens experimentally registered after long-term tests (45 min) correlate well with the reciprocal surface microhardness and with the magnitudes of W_L and W_P estimated using Archard–Rabinowicz formula and complex roughness+strength approach, respectively.
5. In comparison with the original sample, the treated specimens demonstrate the wear losses after short/long-term tests (15/45 min) decreased by 32/68% (after the LHT), by 44/41% (after UIT), and by 52/77% (after the combined LHT + UIT processes).

Acknowledgments

This study is financially supported by the East-West European Network on higher Technical education (EWENT) programme Erasmus Mundus Action 2 Lot 8, as well as partially supported by National Academy of Sciences of Ukraine (Project 0114U001127) and Scientific Program of NASU "Reliability and durability of materials, structures, equipment and buildings Resource 2" (Projects 9.8.1 and 9.8.2).

References

1. J.R. Davis, Surface Hardening of Steels: Understanding the Basics, ASM International, Materials Park, 2002
2. S. Momeni and W. Tillmann, Investigation of the Self-healing Sliding Wear Characteristics of NiTi-Based PVD Coatings on Tool Steel, *Wear*, 2016, **368–369**, p 53–59
3. V. Kovalenko, Ways to Intensify Laser Hardening Technology, *CIRP Ann. Manuf. Technol.*, 1998, **47**(1), p 133–136
4. A.F.I. Idan, O. Akimov, L. Golovko, O. Goncharuk, and K. Kostyk, The Study of the Influence of Laser Hardening Conditions on the Change in Properties of Steels, *East. Eur. J. Eenter. Technol.*, 2016, **2/5** (80), p 69–73
5. M.I.S. Ismail and Z. Taha, Surface Hardening of Tool Steel by Plasma Arc with Multiple Passes, *Int. J. Technol.*, 2014, **5**, p 79–87
6. R.G. Song, K. Zhang, and G.N. Chen, Electron Beam Surface Treatment. Part I: Surface Hardening of AISI, D3 Tool Steel, *Vacuum*, 2003, **69**, p 513–516
7. P. Sun, S. Li, G. Yu, X. He, C. Zheng, and W. Ning, Laser Surface Hardening of 42CrMo Cast Steel for Obtaining a Wide and Uniform Hardened Layer by Shaped Beams, *Int. J. Adv. Manuf. Technol.*, 2014, **70**, p 787–796
8. M. Pellizzari and M.G. De Flora, Influence of Laser Hardening on the Tribological Properties of Forged Steel for Hot Rolls, *Wear*, 2011, **271**, p 2402–2411
9. V.S. Kovalenko and L.F. Golovko, The Role of Dimensional Factors and Absorption Efficiency in Laser Surface Hardening, *Opt. Lasers Eng.*, 1990, **12**(1), p 55–65
10. A. Rodriguez, L.N. Lopez de Lacalle, A. Celaya, A. Lamikiz, and J. Albizuri, Surface Improvement of Shafts by the Deep Ball-Burnishing Technique, *Surf. Coat. Technol.*, 2012, **206**, p 2817–2824
11. P. Balland, T. Laurent, D. Fabien, and M. Vincent, An Investigation of the Mechanics of Roller Burnishing Through Finite Element Simulation and Experiments, *Int. J. Mach. Tools Manufact.*, 2013, **65**, p 29–36
12. C. Nouguier-Lehon, M. Zarwel, C. Diviani, D. Hertz, H. Zahouani, and T. Hoc, Surface Impact Analysis in Shot Peening Process, *Wear*, 2013, **302**, p 1058–1063
13. M. Yasuoka, P. Wang, K. Zhang, Z. Qiu, K. Kusaka, Y. Pyoun, and R. Murakami, Improvement of the Fatigue Strength of SUS304 Austenite Stainless Steel Using Ultrasonic Nanocrystal Surface Modification, *Surf. Coat. Technol.*, 2013, **218**, p 93–98
14. B.N. Mordyuk, O.P. Karasevskaya, and G.I. Prokopenko, Structurally Induced Enhancement in Corrosion Resistance of Zr-2.5%Nb Alloy in Saline Solution by Applying Ultrasonic Impact Peening, *Mater. Sci. Eng., A*, 2013, **559**, p 453–461
15. B.N. Mordyuk, and G.I. Prokopenko, Ultrasonic Impact Treatment—An Effective Method for Nanostructuring the Surface Layers in Metallic Materials. In. M. Aliofkhazraei (Ed.), Handbook of Mechanical Nanostructuring, Wiley-VCH, Weinheim, 2015, p 417-434
16. B.N. Mordyuk and G.I. Prokopenko, Fatigue Life Improvement of α-Titanium By Novel Ultrasonically Assisted Technique, *Mater. Sci. Eng., A*, 2006, **437**, p 396–405
17. Kh.M. Rakhimyanov, K.Kh. Rakhimyanov, A.Kh. Rakhimyanov, and A.V. Kutyshkin, Techniques for Setting Modes of Thermal and Deformation Effect at Combined Hardening and Finishing Operations. *IOP Conference Series: Material Science Engineering*, 2016, **126**, p 012015
18. D.A. Lesyk, S. Martinez, B.N. Mordyuk, V.V. Dzhemelinskyi, A. Lamikiz, G.I. Prokopenko, YuV Milman, and K.E. Grinkevych, Microstructure Related Enhancement in Wear Resistance of Tool Steel AISI, D2 by Applying Laser Heat Treatment Followed by Ultrasonic Impact Treatment, *Surf. Coat. Technol.*, 2017, **328**, p 344–354
19. D.A. Lesyk, S. Martinez, V.V. Dzhemelinskyi, A. Lamikiz, B.N. Mordyuk, and G.I. Prokopenko, Surface Microrelief and Hardness of Laser Hardened and Ultrasonically Peened AISI, D2 Tool Steel, *Surf. Coat. Technol.*, 2015, **278**, p 108–120
20. R. Kumar, S. Kumar, B. Prakash, and A. Sethuramiah, Assessment of Engine Liner Wear From Bearing Area Curves, *Wear*, 2000, **239**, p 282–286
21. G.P. Petropoulos, A.A. Torrance, and C.N. Pandazaras, Abbott Curves Characteristics of Turned Surfaces, *Int. J. Mach. Tools Manuf.*, 2003, **43**, p 237–243
22. S. Martinez, A. Lamikiz, E. Ukar, A. Calleja, J.A. Arrizubieta, and L. N. Lopez de Lacalle, Analysis of the Regimes in the Scanner-Based Laser Hardening Process, *Opt. Lasers Eng.*, 2017, **200**, p 72–80
23. S. Martinez, A. Lamikiz, E. Ukar, I. Tabernero, and I. Arrizubieta, Control Loop Tuning by Thermal Simulation Applied to the Laser Transformation Hardening with Scanning Optics Process, *Appl. Thermal Eng.*, 2016, **98**, p 49–60
24. L.F. Golovko and S.O. Lukyanenko, *Лазерні технології та комп'ютерне моделювання (Laser technology and computer simulation)*, Vistka, Kyiv, 2009 (in Ukrainian)
25. S. Martinez, D.A. Lesyk, A. Lamikiz, E. Ukar, and V.V. Dzhemelinsky, Hardness Simulation of Over-Tempered Area During Laser Hardening Treatment, *Phys. Procedia*, 2016, **83**, p 1357–1366
26. S. Santhanakrishnan, F. Kong, and R. Kovacevic, An Experimentally Based Thermo-Kinetic Phase Transformation Model for Multi-Pass Laser Heat Treatment by Using High Power Direct Diode Laser, *Int. J. Adv. Manuf. Technol.*, 2013, **64**, p 219–238
27. V.V. Dzhemelinskyi and D.A. Lesyk, Визначення оптимальних параметрів лазерно-ультразвукового зміцнення та оздоблювання поверхонь виробів (Determining the Optimal Parameters of Laser-Ultrasonic Hardening and Finishing of the Surface Products), *Bull. NTUU "KPI" Mech. Eng.*, 2013, **68**(2), p 15–18 (in Ukrainian)
28. R. Licek and A. Popov, Evaluation of Selected Parameters of Structural Quality Steel Turning, *Struct. Manuf. Ind. Eng.*, 2012, **11**(2), p 16–19
29. R. Laheurte, P. Darnis, N. Darbois, O. Cahuc, and J. Neauport, Subsurface Damage Distribution Characterization of Ground Surfaces Using Abbott-Firestone, *Opt. Express*, 2012, **20**(12), p 13551–13559
30. B.N. Mordyuk, G.I. Prokopenko, YuV Milman, M.O. Iefimov, K.E. Grinkevych, A.V. Sameljuk, and I.V. Tkachenko, Wear assessment of Composite Surface Layers in Al-6 Mg Alloy Reinforced with AlCuFe

Quasicrystalline Particles: Effects of Particle Size, Microstructure and Hardness, *Wear*, 2014, **319**, p 84–95
31. Y.V. Mil'man, H.M. Nykyforchyn, K.E. Hrinkevych, O.T. Tsyrul'nyk, I.V. Tkachenko, and V.A. Voloshyn, Assessment of the In-Service Degradation of Pipeline Steel by Destructive and Nondestructive Methods, *Mater. Sci.*, 2012, **47**, p 583–589
32. A.G. Suslov, *Инженерия поверхности деталей (Surface Engineering of Parts)*, Machine building, Moscow, 2008 (in Russian)
33. V.V. Stupnytskyy and E.M. Mahorkin, Tribological Criterion of Functional-Oriented Technology of Parts in Engineering, Collected Works of Lutsk National Technical University, *Res. Notes*, 2013, **42**, p 305–313
34. J.R. Clark and M.B. Grant, The Effect of Surface Finish on Component Performance, *Int. J. Mach. Tools Manuf.*, 1992, **32**(1/2), p 57–66
35. A. Zmitrowicz, Wear Patterns and Laws of Wear—A Review, *J. Theor. Appl. Mech.*, 2006, **44**(2), p 219–253
36. I.V. Kragelsky, *Tribology: Lubrication, Friction and Wear*, Wiley, Bury St Edmunds, 2005
37. L. Zhou, G. Liu, Z. Han, and K. Lu, Grain Size Effect on Wear Resistance of a Nanostructured AISI52100 steel, *Scripta Mater.*, 2008, **58**, p 445–448
38. R. Autay, M. Kchaou, K. Elleuch, and F. Dammak, Tribological Behaviour of Carbon and Low Alloy Steels: Effect of Mechanical Properties and Test Conditions, *Tribology*, 2011, **5**(4), p 133–140
39. W. Koszela, A. Dzierwa, L. Galda, and P. Pawlus, Experimental Investigation of Oil Pockets Effect on Abrasive Wear Resistance, *Tribol. Int.*, 2012, **46**(1), p 145–153
40. K. Zaleski and A. Skoczylas, Effect of Vibration Shot Peening Parameters Upon Shapes of Bearing Curves of Alloy Steel Surface, *Adv. Sci. Technol. Res. J.*, 2015, **9**(25), p 20–26
41. J. Zhang, W. Li, H. Wang, Q. Song, L. Lu, W. Wang, and Z. Liu, A Comparison of the Effects of Traditional Shot Peening and Micro-Shot Peening on the Scuffing Resistance of Carburized and Quenched Gear Steel, *Wear*, 2016, **368–369**, p 253–257
42. A.M. El-Batahgy, R.A. Ramadan, and A.R. Moussa, Laser Surface Hardening of Tool Steels—Experimental and Numerical Analysis, *J. Surf. Eng. Mater. Adv. Technol.*, 2013, **3**(02), p 146–153
43. E. Ukar, A. Lamikiz, L.N. Lopez de Lacalle, D. de l Pozo, and J.L. Arana, Laser Polishing of Tool Steel with CO_2 Laser and High-Power Diode Laser, *Int. J. Mach. Tools Manuf.*, 2010, **50**, p 115–125
44. W. Guo, M. Hua, P. Wai-Tat Tse, and A. Chiu Kam Mok, Process Parameters Selection for Laser Polishing DF2 (AISI, O1) by Nd:YAG Pulsed Laser Using Orthogonal Design, *Int. J. Manuf. Technol.*, 2012, **59**, p 1009–1023
45. F.A. Goia and M.S. Fernandes de Lima, Surface Hardening of an AISI, D6 Cold Work Steel Using a Fiber Laser, *J. ASTM Int.*, 2011, **8**, p 1–9
46. G.D. Gureev and D.M. Gureev, Совмещение лазерного и ультразвукового воздействий для термообработки поверхности стали (The combination of laser and Ultrasonic Action For Heat Treatment of Steel Surface), *Vestnik Samara State Univ.*, 2007, **14**(1), p 90–95 ((in Russian))
47. J.H. Lee, J.H. Jang, B.D. Joo, Y.M. Son, and Y.H. Moon, Laser Surface Hardening of AISI, H13 Tool Steel, *Trans. Nonferrous Met. Soc. China*, 2009, **19**, p 917–920
48. N. Yasavol, A. Abdollah-zadeh, M. Ganjali, and S.A. Alidokht, Microstructure and Mechanical Behavior of Pulsed Laser Surface Melted AISI, D2 Cold Work Tool Steel, *Appl. Surf. Sci.*, 2013, **265**, p 653–662
49. S. Mitrovic, D. Adamovic, F. Zivic, D. Dzunic, and M. Pantic, Friction and Wear Behavior of Shot Peened Surfaces of 36CrNiMo4 and 36NiCrMo16 Alloyed Steels Under Dry and Lubricated Contact Conditions, *Appl. Surf. Sci.*, 2014, **290**, p 223–232
50. A. Amanov, I.S. Cho, Y.S. Pyoun, C.S. Lee, and I.G. Park, Micro-Dimpled Surface by Ultrasonic Nanocrystal Surface Modification and its Tribological Effects, *Wear*, 2012, **286–287**, p 136–144